



Phytoplankton Growth and Productivity in the Western North Atlantic: Observations of Regional Variability From the NAAMES Field Campaigns

James Fox¹, Michael J. Behrenfeld², Nils Haëntjens³, Alison Chase³, Sasha J. Kramer^{4,5}, Emmanuel Boss³, Lee Karp-Boss³, Nerissa L. Fisher¹, W. Bryce Penta¹, Toby K. Westberry¹ and Kimberly H. Halsey^{1*}

OPEN ACCESS

Edited by:

Dongyan Liu,
East China Normal University, China

Reviewed by:

Timothy James Smyth,
Plymouth Marine Laboratory,
United Kingdom
Fang Shen,
East China Normal University, China

*Correspondence:

Kimberly H. Halsey
halseyk@science.oregonstate.edu

Specialty section:

This article was submitted to
Marine Ecosystem Ecology,
a section of the journal
Frontiers in Marine Science

Received: 06 November 2019

Accepted: 14 January 2020

Published: 07 February 2020

Citation:

Fox J, Behrenfeld MJ,
Haëntjens N, Chase A, Kramer SJ,
Boss E, Karp-Boss L, Fisher NL,
Penta WB, Westberry TK and
Halsey KH (2020) Phytoplankton
Growth and Productivity
in the Western North Atlantic:
Observations of Regional Variability
From the NAAMES Field Campaigns.
Front. Mar. Sci. 7:24.
doi: 10.3389/fmars.2020.00024

¹ Department of Microbiology, Oregon State University, Corvallis, OR, United States, ² Department of Botany and Plant Pathology, Oregon State University, Corvallis, OR, United States, ³ School of Marine Sciences, University of Maine, Orono, ME, United States, ⁴ Department of Geography, University of California, Santa Barbara, Santa Barbara, CA, United States, ⁵ Earth Research Institute, University of California, Santa Barbara, Santa Barbara, CA, United States

The ability to quantify spatio-temporal variability in phytoplankton growth and productivity is essential to improving our understanding of global carbon dynamics and trophic energy flow. Satellite-based observations offered the first opportunity to estimate depth-integrated net primary production (NPP) at a global scale, but early modeling approaches could not effectively address variability in algal physiology, particularly the effects of photoacclimation on changes in cellular chlorophyll. Here, a previously developed photoacclimation model was used to derive depth-resolved estimates of phytoplankton division rate (μ) and NPP. The new approach predicts NPP values that closely match discrete measurements of ¹⁴C-based NPP and effectively captured both spatial and temporal variability observed during the four field campaigns of the North Atlantic Aerosols and Marine Ecosystems Study (NAAMES). We observed favorable growth conditions for phytoplankton throughout the annual cycle in the subtropical western North Atlantic. As a result, high rates of μ are sustained year-round resulting in a strong coupling between growth and loss processes and a more moderate spring bloom compared to the high-latitude subarctic region. Considerable light limitation was observed in the subarctic province during the winter, which resulted in divergent growth dynamics, stronger decoupling from grazing pressure and a taxonomically distinct phytoplankton community. This study demonstrates how detailed knowledge of phytoplankton division rate furthers our understanding of global carbon cycling by providing insight into the resulting influence on phytoplankton taxonomy and the loss processes that dictate the fate of fixed carbon.

Keywords: phytoplankton, NPP, carbon, photoacclimation, modeling, optics, North Atlantic

INTRODUCTION

Despite constituting less than 1% of the earth's photosynthetic biomass, marine phytoplankton are estimated to be responsible for almost half the global annual net primary production (Field et al., 1998). The vast quantity of organic carbon fixed by phytoplankton in the sunlit layer of the ocean provides the primary source of energy for marine food webs and the global phytoplankton community grows, divides, and expires (to grazing or viral lysis) every few days (Behrenfeld and Falkowski, 1997a; Bidle, 2015). Approximately 85–90% of the carbon fixed through primary production in the euphotic zone will remain within the upper ocean, including the twilight zone, where it is remineralized and recycled. The remaining fraction is exported to the deep ocean (Giering et al., 2014) where the organic carbon turnover rate is on the scale of years (and longer) in the mesopelagic and bathypelagic zones (Rowe et al., 1990). Accurately quantifying the spatial and temporal variability in phytoplankton productivity is therefore paramount to improving our understanding of global carbon dynamics and trophic energy flow (Siegel et al., 2014; Boyd et al., 2019).

Assessments of marine primary production and carbon cycling are made difficult by the extreme plasticity in phytoplankton physiology that allows these organisms to exist ubiquitously throughout the sunlit ocean (Geider et al., 1998; Halsey and Jones, 2015). Phytoplankton photosynthesis is limited by the availability of nutrients and light, leading to suppressed growth and productivity in oligotrophic or light-limited environments (Geider et al., 2001; Arrigo, 2005; Moore et al., 2013). To optimize growth in these resource-limited environments, phytoplankton adjust their light harvesting strategy and reallocate photosynthetic energy to different metabolic pathways (Halsey and Jones, 2015). Collectively, these photoacclimatory processes prime phytoplankton for optimal growth in their extant environment and have been extensively studied in laboratory cultures (Laws and Bannister, 1980; Geider et al., 1997; Halsey et al., 2014). When environmental conditions permit, phytoplankton can divide at rates that exceed losses to top-down pressures, resulting in an accumulation of phytoplankton biomass known as “blooming” (Behrenfeld and Boss, 2014). If sustained for sufficient time, these periods of accumulation can result in substantial CO₂ sequestration and organic carbon export, a quintessential example being the large scale springtime blooming event across the subarctic Atlantic ocean (Friedland et al., 2016). Approximately 0.55 to 1.94 Gt C year⁻¹ of the annual global carbon export out of the euphotic zone (~11 Gt C year⁻¹) originates in the North Atlantic Ocean, with roughly half of this occurring during the spring bloom (Sanders et al., 2014; Siegel et al., 2016).

Optical technologies provide the most effective approach to probe phytoplankton dynamics over large scales of space and time. Mounted on platforms including satellites, ships, gliders, floats, and fixed moorings, optical sensors offer a spatially and temporally cohesive picture of phytoplankton biomass and physiology that *in situ* sampling approaches cannot fully resolve (O'Reilly et al., 1998; Boss et al., 2008; Briggs et al., 2018). Bulk properties of chlorophyll concentration (Chl) and, more recently,

phytoplankton biomass (C_{phyto}) have been retrieved from space over the past four decades and are routinely implemented into models to provide global estimates of NPP and carbon export (Antoine et al., 1996; Behrenfeld and Falkowski, 1997a; Smyth et al., 2005; Westberry et al., 2008; Uitz et al., 2010; Silsbe et al., 2016). When combined with ship-based field data, these satellite observations are revealing how environmental and biological factors combine to control global and regional variability in phytoplankton physiology and distribution (Behrenfeld et al., 2006, 2009; Blondeau-Patissier et al., 2014). Similar optics-based approaches to assess primary productivity and export using floats (Estapa et al., 2019), ships (Burt et al., 2018) or remotely operated vehicles (Hemsley et al., 2015; Massicotte et al., 2019) are starting to resolve fine-scale dynamics, such as physiological changes occurring on hourly timescales or distributions of stocks at sub-pixel scales that cannot yet be captured using satellite-based approaches (Bracher et al., 2017). These recent studies highlight the potential efficacy of multi-platform approaches to untangle complex dynamics within the marine carbon cycle, while providing an invaluable opportunity to validate and ground truth satellite-based models.

This report utilizes optical data collected during a multi-year study in the western North Atlantic that targeted key phases of the annual bloom cycle (Behrenfeld et al., 2019). These data provide an opportunity to quantify NPP across a large dynamic range of standing stocks and growth conditions, with specific interest in characterizing underlying changes in phytoplankton biomass and physiology. Use of an existing photoacclimation model accounted for a large amount of variability in the ratio of key proxies of phytoplankton Chl and C_{phyto}, providing new evidence supporting the theory that the depth and duration of the winter mixing period determine the ultimate magnitude of the subsequent spring bloom. We further explore residual variability in optical properties retrievable from space as an avenue for improving remote sensing productivity assessments.

MATERIALS AND METHODS

Ship-based measurements were made onboard the R/V *Atlantis* during the field program (2015–2018) of the North Atlantic Aerosols and Marine Ecosystems Study (NAAMES) (Behrenfeld et al., 2019). An overarching objective of NAAMES was to characterize plankton ecosystem dynamics over the course of an annual cycle and determine the environmental conditions required to produce the annual subarctic phytoplankton bloom. The four field campaigns were structured to align with specific phytoplankton bloom phases, based on the framework of the Disturbance-Recovery Hypothesis (Behrenfeld and Boss, 2018): the *winter transition* (November 2015 campaign) where mixed layer depth (MLD) is deepening and phytoplankton concentration is stable or decreasing, the *accumulation phase* where the MLD begins shoaling and phytoplankton concentration starts to increase (March 2018 campaign), the *bloom climax/transition* where a shallow MLD leads to a recoupling of phytoplankton division and loss rates (May 2016 campaign), and an *equilibrium phase* where

deteriorations in mixed layer growth conditions result in a more stable system where phytoplankton loss rates are proportional to division rates (September, 2017 campaign). This experimental design resulted in extensive variability in observations of phytoplankton biomass, productivity, and physiological conditions over time and space, providing an excellent platform to probe our “skill” in modeling these parameters to understand how the environment and biological processes integrate to yield an annual phytoplankton bloom cycle. All data presented in this report were collected along the primary “science intensive” transect, located between $\sim 40^{\circ}\text{N}$ and $\sim 55^{\circ}\text{N}$ latitude along the 40°W longitude (**Figure 1**). For each campaign, a number of stations were occupied along this transect to allow for water column profiling and acquisition of discrete samples from depth.

Underway Optical Properties

Temperature, salinity and optical properties were measured continuously on the ship’s clean seawater supply (intake at approximately 5 m depth) during all field campaigns. A flow-through system with a diaphragm pump was employed throughout the NAAMES field campaign to avoid unwanted interference with the sampled plankton populations (Cetinić et al., 2016). The seawater was delivered through a vortex debubbler to various optical instruments. A WetLabs ACS was used to measure hyperspectral particulate attenuation and absorption, optical measurements commonly used to estimate Chl concentration (Chl_{ACS}), particulate organic carbon, and particle size index (Boss et al., 2001; Cetinić et al., 2012). The Chl_{ACS} concentrations were derived from the line height of the chlorophyll absorption peak in the

red (Boss et al., 2007) and tuned using the NAAMES high performance liquid chromatography (HPLC) samples collected underway (Eq. 1). A WetLabs ECO-BB3 was used to measure the angular scatterance at 1 Hz at three wavelengths (470, 532, and 660 nm). The optical measurements use a calibration-independent technique (Slade et al., 2010) by differencing filtered measurements ($0.2 \mu\text{m}$) from total measurements (no filter).

$$\begin{cases} a_{\varphi} = a_{p(676)} - \left(\frac{36}{65}a_{p(650)} + \frac{26}{65}a_{p(715)}\right) \\ \text{Chl}_{\text{ACS}} = 95 a_{\varphi}^{1.06} \end{cases} \quad (1)$$

Optically-derived estimates of phytoplankton biomass ($C_{\text{phyto}}^{\text{bbp}}$) were calculated using particulate backscatter at the 470 nm wave band ($b_{\text{bp}(470)}$) following Graff et al. (2015) according to Eq. 2:

$$C_{\text{phyto}}^{\text{bbp}} = b_{\text{bp}(470)} \cdot 12129 + 0.67 \quad (2)$$

Modeling Phytoplankton Growth and Productivity

Phytoplankton acclimate to changing environmental conditions through a number of physiological responses. Laboratory and field observations of C_{phyto} to Chl ratios (θ ; see **Table 1** for a full listing of symbols, terms, definitions and units) follow anticipated physiological dependencies on light (photoacclimation), nutrients and temperature, which in turn can be used to estimate phytoplankton growth rate. Phytoplankton communities that encounter a significant decrease in growth irradiance (under nutrient replete conditions) will typically increase cellular Chl resulting in a decrease in θ (**Figure 2A**), which is paralleled by a decrease in growth rate. The opposite behavior is observed

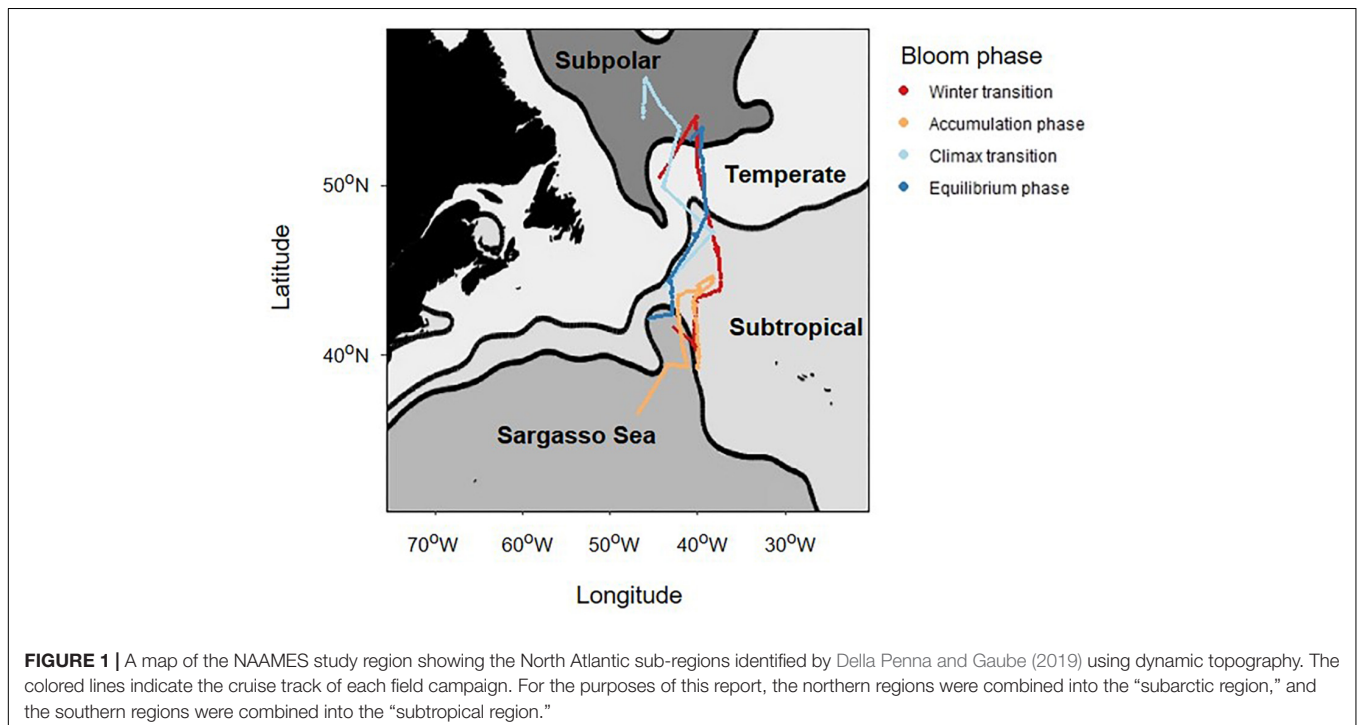


TABLE 1 | Symbols, terms, definitions and units.

Symbol	Description
NAAMES	The North Atlantic Aerosol and Marine Ecosystem Study
NPP (^{14}C)	Net primary production measured using ^{14}C ($\text{mg C m}^{-2} \text{d}^{-1}$)
f_{μ}	Phytoplankton division rate calculated for the surface mixed layer (d^{-1})
f_{NPP}	Modeled net primary production integrated through the euphotic zone ($\text{mg C m}^{-2} \text{d}^{-1}$)
$f_{\text{NPP}_{\text{MLD}}}$	Modeled net primary production integrated through the mixed layer ($\text{mg C m}^{-2} \text{d}^{-1}$)
I_g	Median mixed layer growth irradiance (moles of photons $\text{m}^{-2} \text{hr}^{-1}$)
Chl_{ACS}	Chlorophyll estimated from fluorescence line height (mg C m^{-3})
b_{bp}	Particulate backscatter
C_{phyto}	Phytoplankton biomass (mg C m^{-3})
$C_{\text{phyto}}^{\text{bbp}}$	Observed estimates of C_{phyto} derived from particulate backscatter (mg C m^{-3})
$C_{\text{phyto}}^{\text{mod}}$	Modeled estimates of C_{phyto} derived from the photoacclimation model and Chl_{ACS} (mg C m^{-3})
θ	$C_{\text{phyto}}:\text{Chl}$
θ_{opt}	$C_{\text{phyto}}^{\text{bbp}}:\text{Chl}_{\text{ACS}}$
θ_{PaM}	$C_{\text{phyto}}:\text{Chl}$ modeled using a photoacclimation model (equations (3) and (5))
PAR	Photosynthetically active radiation (moles of photons $\text{m}^{-2} \text{hr}^{-1}$)

during shallow mixing, where pigmentation often decreases due to the combined influences of high-light acclimation and nutrient limitation (**Figure 2B**). Through our understanding of the mechanisms of photoacclimation and the environmental drivers that alter θ , it is possible to estimate growth rate and NPP.

A previously developed photoacclimation model (PaM) (Behrenfeld et al., 2016) is used here to estimate θ along the full science-intensive transect during each of the four NAAMES field campaigns. The PaM is composed of a “baseline” deep-mixing solution (θ_{DM}) and a shallow-mixing correction ($\Delta\theta_{\text{SM}}$), such that for any given mixing depth $\theta_{\text{PaM}} = \theta_{\text{DM}} + \Delta\theta_{\text{SM}}$.

A fundamental concept introduced in the development of the PaM was that molecular signals regulating chlorophyll synthesis are influenced during exposure to darkness, such that chlorophyll synthesis abates. The model assumes that this dark condition occurs at depths greater than six optical depths and that the value of θ_{PaM} for all mixing depths greater than this horizon is described by θ_{DM} (that is $\Delta\theta_{\text{SM}}$ has a value of 1):

$$\theta_{\text{DM}} = 19 \cdot e^{\left(0.038 \cdot \frac{\text{PAR}^{0.45}}{K_d}\right)} \quad (3)$$

where PAR is the photosynthetically active radiation flux ($400\text{--}700 \text{ nm}$, $\text{mol photons m}^{-2} \text{h}^{-1}$), which for the current study was measured (1 min resolution) using a Licor Model LI-189 cosine sensor, and K_d is the attenuation coefficient for downwelling PAR estimated from Chl_{ACS} concentrations (Morel et al., 2007):

$$K_d = 0.0166 + 0.0773 \cdot \text{Chl}_{\text{ACS}}^{0.6715} \quad (4)$$

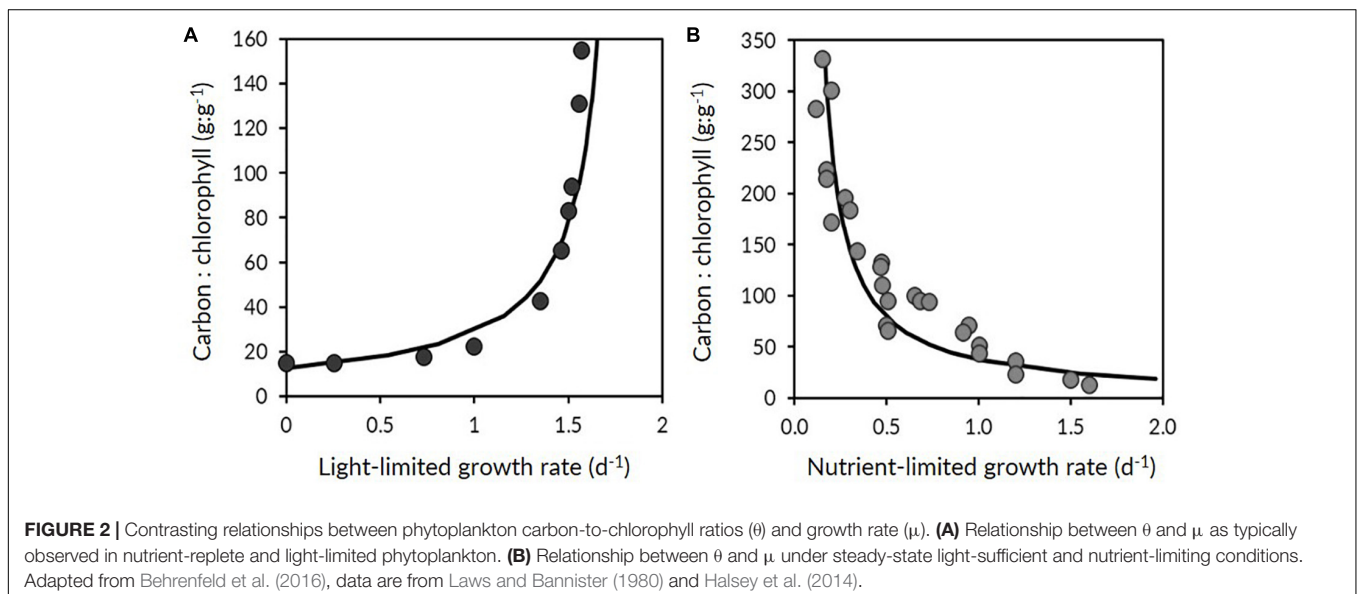
For mixed layers less than six optical depths, a shallow mixing correction is added ($\Delta\theta_{\text{SM}}$) and calculated as:

$$\Delta\theta_{\text{SM}} = \frac{1 + e^{(-0.15 \cdot \text{PAR})}}{1 + e^{(-3 \cdot I_g)}} \quad (5)$$

where I_g is the median growth irradiance in the surface mixed layer:

$$I_g = \text{PAR} \cdot e^{(-0.5 \cdot K_d \cdot \text{MLD})} \quad (6)$$

Herein, MLD is estimated using a dynamic threshold method based on Brunt Väisälä frequency (N^2). The N^2 -based estimates of MLD were calculated from CTD profiles (carried out every $1\text{--}3 \text{ day}^{-1}$) and defined as the depth ($>5 \text{ m}$) at which N^2 increased to a value greater than the absolute value of the standard deviation of the unsmoothed (raw) N^2 profile. The discrete estimates of MLD were then linearly interpolated between casts to derive MLD for the full science intensive



transect. For further details on NAAMES MLD calculations see Graff and Behrenfeld (2018).

Daily averages of θ_{PaM} for each station were then derived from the transect data and used to calculate depth-resolved estimates of phytoplankton division rate and NPP. All transect data between stations were omitted from the NPP analysis to remove the variability in model estimates driven by changes in MLD, which were not measurable when in transit. Components of the PaM (Eqs 3 and 5) were used to infer phytoplankton division rate (μ) using published relationships between μ and θ from field and laboratory studies (Figure 2):

$$\mu = \left[\left(\frac{1}{\theta_{DM}} (-16.80) + 1.57 \right) \cdot \left(\frac{1}{\theta_{PaM}} (47.03) + 0.0125 \right) \right] \cdot [1 - e^{(-5 \cdot PAR(z))}] \quad (7)$$

here the final term describes the reduction in growth rate as a result of decreasing ambient light estimated iteratively with depth. The decrease reflects the inability of photoacclimation to maintain sufficient light absorption at all light levels. The strength of the light limitation effect on μ is characterized by the exponent (-5) in Eq. 7 (Westberry et al., 2008).

θ_{PaM} was multiplied by Chl_{ACS} to yield phytoplankton biomass (C_{phyto}^{mod}) which is assumed to be uniform throughout the photic layer (Westberry et al., 2008). Depth-resolved NPP was calculated as $\mu \times C_{phyto}^{mod}$ at each depth increment. Depth-integrated μ ($\int \mu$) for the mixed layer was calculated as:

$$\int \mu = \frac{\int NPP_{MLD}}{\int C_{phyto}^{mod}} \quad (8)$$

where $\int NPP_{MLD}$ and C_{phyto}^{mod} are the values of NPP and modeled C_{phyto} integrated through the surface mixed layer. Discrete measurements of NPP determined using 24 h ^{14}C -uptake (see below) were used to ground-truth modeled productivity values. Means from different sampling locations and regions were compared using a one-way analysis of variance (ANOVA) and *post hoc* Tukey-Kramer (T-K) test when necessary ($\alpha = 0.05$).

Net Primary Production Measurements

NPP was determined using ^{14}C uptake incubations. Water collected pre-dawn from 4 to 5 depths was inoculated with ^{14}C -labeled sodium bicarbonate and incubated in on-deck incubators at light levels corresponding to the collection depths. Following incubation (24 h, dawn-to-dawn), samples were filtered onto 0.2 μm polycarbonate membrane filters, acidified with 1 M HCl and allowed to degas for 24 h. 10 ml of liquid scintillation cocktail were added to each sample before measuring activity with a scintillation counter. Prior to incubations, three 100 μL subsamples were collected immediately following the " ^{14}C -spike" to accurately measure total activity of ^{14}C -labeled sodium bicarbonate added to each sample. These samples were mixed with 50 μL of β -phenylethylamine and scintillation cocktail before measurement in the scintillation counter.

Phytoplankton Pigment Composition

Water samples (1–3 L) for phytoplankton pigment composition were collected from surface (5 m) Niskin bottles or the ship's underway water supply and filtered through 25 mm GF/F filters. Filters were flash-frozen and stored in liquid nitrogen until analysis. Samples were analyzed using HPLC at the NASA Goddard Space Flight Center Ocean Ecology Laboratory following established protocols (Van Heukelem and Thomas, 2001). Degradation products and redundant accessory pigments were removed from the dataset, leaving sixteen pigments for analysis: 19'-hexanoyloxyfucoxanthin, 19'-butanoyloxyfucoxanthin, alloxanthin, fucoxanthin, peridinin, diatoxanthin, diadinoxanthin, zeaxanthin, divinyl chlorophyll a, monovinyl chlorophyll b, divinyl chlorophyll b, chlorophyll $c_1 + c_2$, chlorophyll c_3 , neoxanthin, violaxanthin, and prasinoxanthin. Lutein (an accessory pigment found in green algae) was also removed from the dataset, as it was undetected in >75% of samples. All pigments were normalized to total Chl *a* concentration before a network-based community detection analysis was performed following the methods of Kramer et al. (in review) to identify the taxonomic community to which each sample was assigned following a data-driven network-based community detection analysis.

Briefly, in the network-based community detection analysis, each sample becomes a node in the network; the edges connecting each sample to all other samples are described by the strength of the correlation between the sites. The HPLC pigment dataset is first transformed into a symmetrical adjacency matrix that describes the Pearson's correlation coefficient between every set of samples based on the ratios of all sixteen pigments to total Chl *a*. The edges between samples were weighted following the Weighted Gene Co-Expression Network Analysis (WGCNA; Zhang and Horvath, 2005) before the community detection analysis was performed on the adjacency matrix. The community detection algorithm identified five distinct taxonomic communities based on the concentrations of pigments in each community: cyanobacteria, diatom, dinoflagellate, green algae/mixed population, and haptophyte.

RESULTS

Evaluation of broad scale variability in mean dynamic topography allowed the NAAMES study region to be classified into four defined provinces (Figure 1): subarctic, temperate, subtropical, and Sargasso Sea/Gulf Stream (Della Penna and Gaube, 2019). Based on similarities in physical-chemical properties and highly-defined phytoplankton community composition, we grouped subarctic and temperate provinces together and subtropical and Sargasso Sea provinces together following the approach of Bolanos et al. (in review). These broader groups are hereafter referred to as the subarctic and subtropical regions, respectively.

Water column stratification and upper ocean mixing dynamics showed strong seasonality across the four campaigns. During the *winter transition* (November), northern stations in the subarctic region exhibited a well-mixed upper layer >60 m

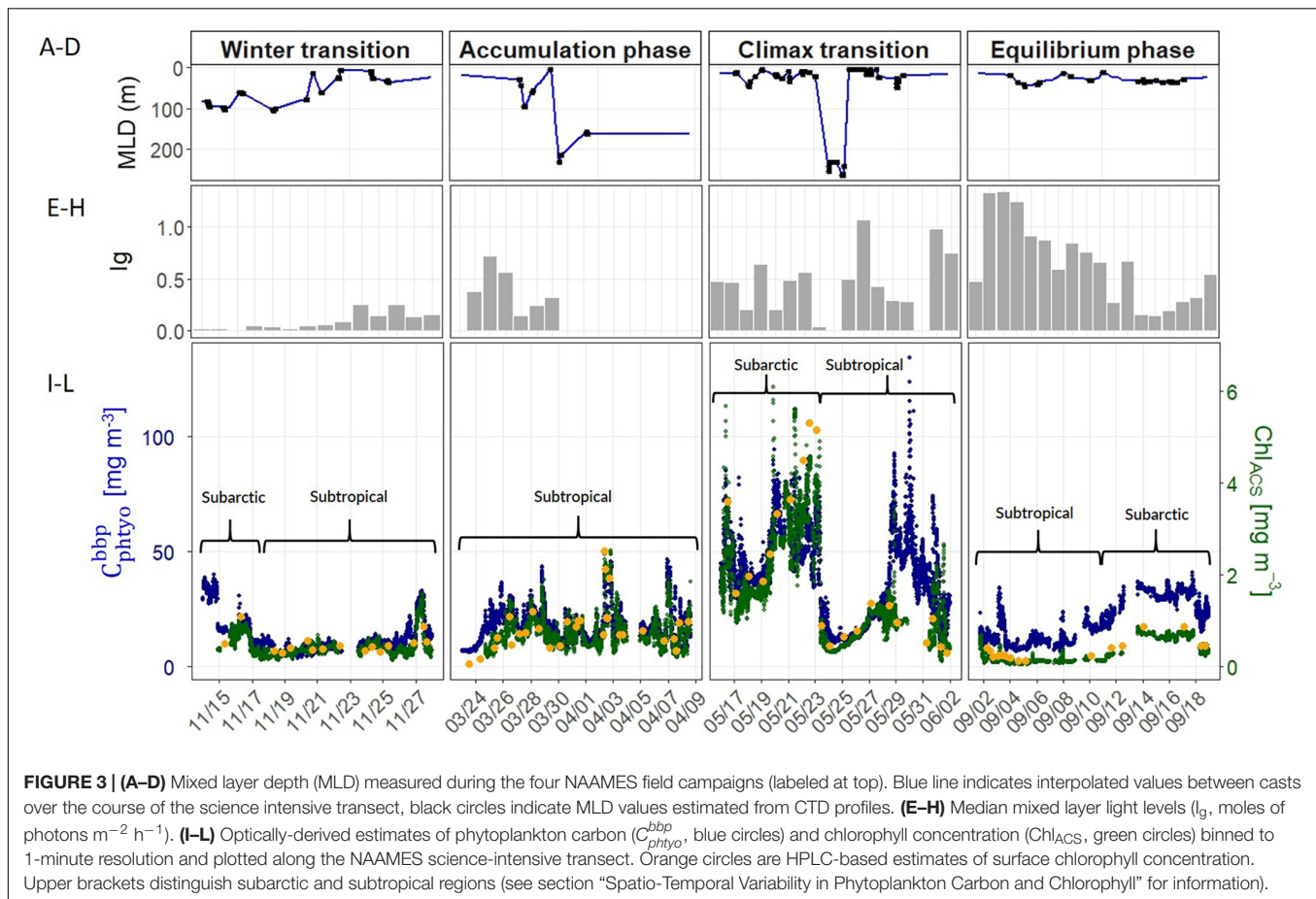


(Figure 3A). As the ship progressed further south into the subtropical region, the water column became more stratified with a shallow MLD (<25 m). All stations sampled during the *accumulation phase* (March) were located south of $45^{\circ}N$ in the subtropical region, where the degree of stratification varied extensively and the MLD ranged from 6 to 231 m (Table 2 and Figure 3B). Water column conditions during the *climax transition* (April–May; Figure 3C) and *equilibrium phase* (August–September; Figure 3C) were characterized by strong thermal stratification and mixed layers shallower than 35 m, with one exception during the climax transition being a strong physical disturbance where the water column was temporarily homogenized to a depth of ~ 200 m immediately before arrival at one of the sampling stations ($47^{\circ}39.360N$, $39^{\circ}11.398W$) (Graff and Behrenfeld, 2018).

Spatio-Temporal Variability in Phytoplankton Carbon and Chlorophyll

Annual cycles of mixing, stratification, and light availability (Figures 3A–H) yielded minimum C_{phyto} and Chl concentrations in winter, an accumulation of phytoplankton biomass in spring reaching a late spring climax, followed by an autumn decline in both properties in the subarctic and subtropical regions (Figures 3I–L). One difference between the two regions is

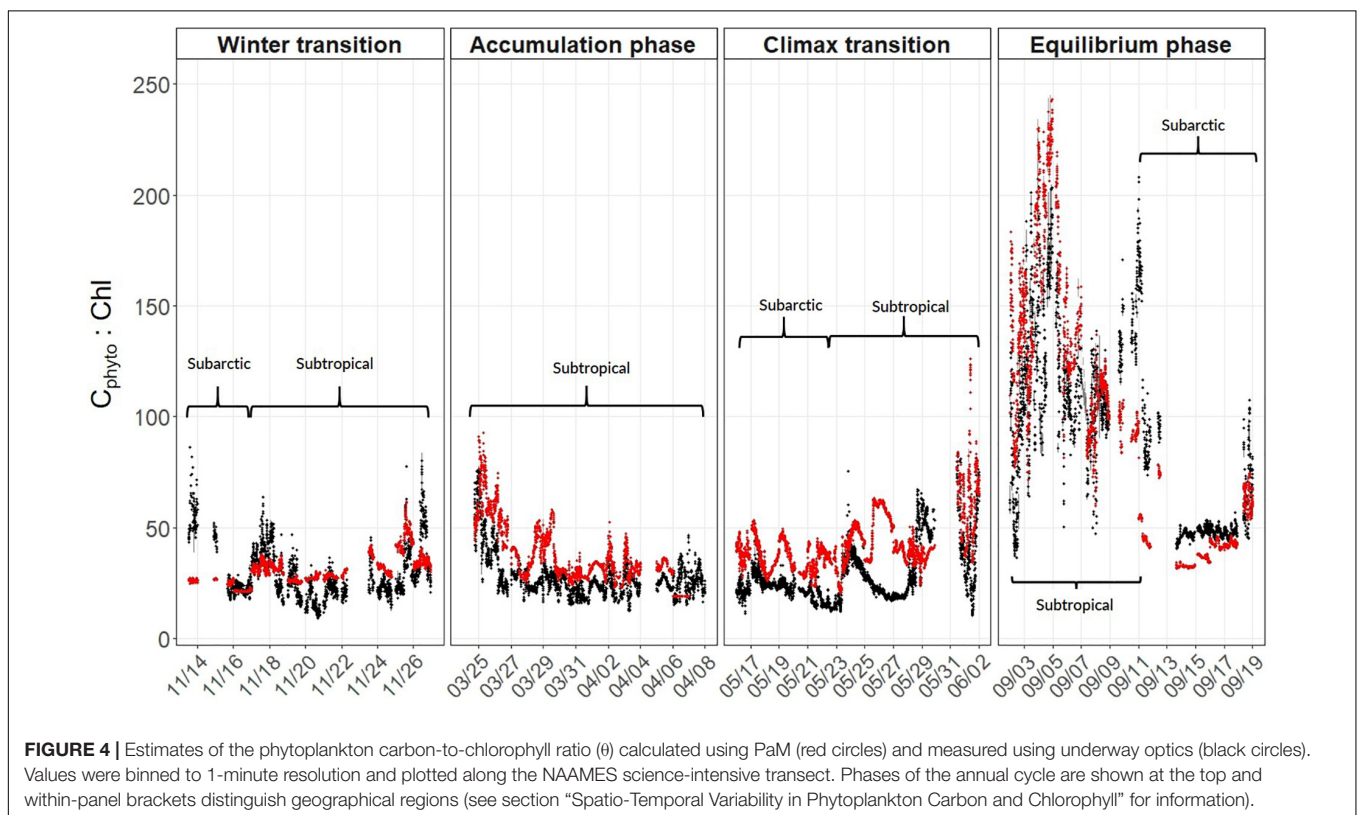
that the subarctic climax biomass appeared slightly elevated compared to subtropical levels (Figure 3K). Both the optically-derived (Chl_{ACS}) and discrete surface measurements of Chl (HPLC from 5 m) effectively captured the spatial and temporal heterogeneity observed during each campaign (Figures 3I–L). The high temporal resolution (1 min bins) of the underway optical instruments revealed tightly coupled patterns in C_{phyto}^{bbp} and Chl_{ACS} ratios (Figures 3I–L). Nevertheless, measured C_{phyto}^{bbp} to Chl_{ACS} ratios (θ_{opt}) exhibited a 20-fold range in variability (10 – 235 $mg\ m^{-3} : mg\ m^{-3}$) across the four field campaigns (Figure 4). This large range was dominated by the *equilibrium phase* (average θ_{opt} of 94 ± 43) (Figure 4) when light intensity was at the highest and nitrate (N) concentrations were significantly lower (ANOVA, T-K, $p < 0.01$) as indicated by N:P (Table 2). Values of θ_{opt} during the other three campaigns (*winter transition*, *accumulation phase* and *climax transition*) were substantially lower and remarkably similar (28 ± 11 , 27 ± 10 , 27 ± 11 $mg\ m^{-3} : mg\ m^{-3}$, respectively), with the low averages indicating growth conditions in the surface mixed layer were predominantly light-limiting and nutrient-replete.

Field-measured θ_{opt} values exhibited good agreement with θ_{PaM} for the full science-intensive transect of the four field campaigns ($y = 0.85x + 12.34$, $r^2 = 0.72$, $RMSE = 19.17$) (Figure 4 and Supplementary Figure S1). The ability of the

TABLE 2 | Mean and standard deviation, maximum and minimum values of physical, biological and chemical parameters measured during the four NAAMES field campaigns.

	NAAMES 1 11/6/15–12/1/15 “winter transition”			NAAMES 4 03/20/18–4/13/18 “accumulation phase”			NAAMES 2 05/11/16–6/5/16 “climax transition”			NAAMES 3 08/30/17–9/24/17 “equilibrium phase”		
	Min	Max	Mean ± SD	Min	Max	Mean ± SD	Min	Max	Mean ± SD	Min	Max	Mean ± SD
MLD	7	107	58 ± 33	6	231	110 ± 76	5	264	55 ± 85	13	46	33 ± 8
K_d	0.03	0.10	0.05 ± 0.01	0.04	0.16	0.07 ± 0.01	0.05	0.28	0.11 ± 0.04	0.02	0.09	0.04 ± 0.02
N:P	1.6	18.6	12.0 ± 5.7	4.7	28.3	9.7 ± 5.5	5.2	24.2	16.2 ± 4.8	0.2	24.0	5.9 ± 4.9
HPLC Chl	0.27	1.07	0.43 ± 0.20	0.14	2.50	0.90 ± 0.55	0.43	5.30	2.32 ± 1.61	0.10	0.85	0.33 ± 0.24
Chl _{ACS}	0.11	1.06	0.38 ± 0.17	0.18	2.52	0.69 ± 0.31	0.28	6.15	1.52 ± 1.11	0.03	0.88	0.32 ± 0.27
POC	8.0	302.4	61.5 ± 64.0	23.7	174.8	72.2 ± 32.4	31.3	534.9	172.6 ± 105.9	12.2	292.6	72.6 ± 48.4
C_{phyto}^{bbp}	3.0	47.9	12.09 ± 7.88	6.9	56.1	17.97 ± 6.76	9.6	150.3	39.07 ± 19.96	5.8	41.5	19.67 ± 10.14

MLD, mixed layer depth; K_d , the light attenuation coefficient; N:P, Nitrogen to phosphorus ratio; HPLC Chl, Chlorophyll a measured by HPLC; Chl_{ACS}, Optically-derived estimates of chlorophyll a; POC, Particulate organic carbon; C_{phyto}^{bbp} , Estimates of phytoplankton carbon derived using particulate backscatter (b_{bp}).



PaM, which only accounts for physiological light responses, to reproduce the mixed layer observations suggests that light-driven photoacclimation was the dominant driver of θ variability (Figure 4). To examine secondary drivers of the remaining unexplained θ variance, we explored influences of phytoplankton community composition on particulate backscatter by comparing it against modeled estimates of carbon. Measurements of θ_{PaM} and Chl_{ACS} both correlated strongly with θ_{opt} and HPLC observations, respectively ($r^2 = 0.72$ and 0.95), giving confidence in the C_{phyto}^{mod} values. For NAAMES, comparison of $b_{bp(470)}$ and C_{phyto}^{mod} yielded a linear regression slope ($r^2 = 0.60$, $y = 14760x + 0.72$) that was similar to previously published

values (Behrenfeld et al., 2005; Graff et al., 2015; Figure 5). This finding suggests that variability in phytoplankton community composition, outside of its influence on the particle size distribution, played a significant role in observed θ_{opt} variability, particularly during the *climax transition* when θ_{opt} and θ_{PaM} showed the poorest match ups (Figure 4).

Modeled Phytoplankton Growth and Primary Production

The vast majority of modeled estimates of NPP showed good agreement with measurements from 24 h ^{14}C -uptake bottle incubations ($r^2 = 0.80$, $y = 0.99x - 1.4$, RMSE = 6.03,

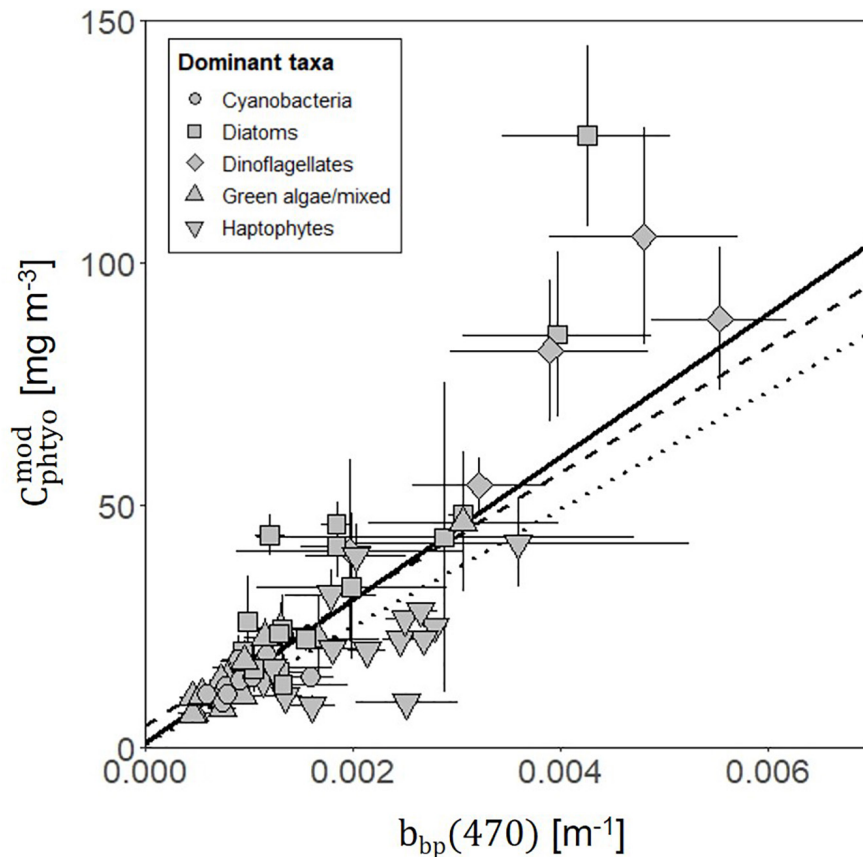


FIGURE 5 | Relationship between modeled phytoplankton carbon ($C_{\text{phyto}}^{\text{mod}}$) values (derived from θ_{PaM} and Chl_{ACS}) and measurements of particulate backscatter ($b_{\text{bp}}(470)$) (solid line; $y = 14910x + 0.70$, $r^2 = 0.61$, $\text{RMSE} = 16.31$) along the full science intensive transect from all four campaigns. Points show daily mean with error bars indicating standard deviations. Symbol shape indicates the dominant phytoplankton within the community, estimated using a community detection algorithm. Previously published relationships are also shown from Behrenfeld et al. (2005) (dashed line; $y = 13000x + 4.55$) and Graff et al. (2015) (dotted line; $y = 12128x + 0.59$).

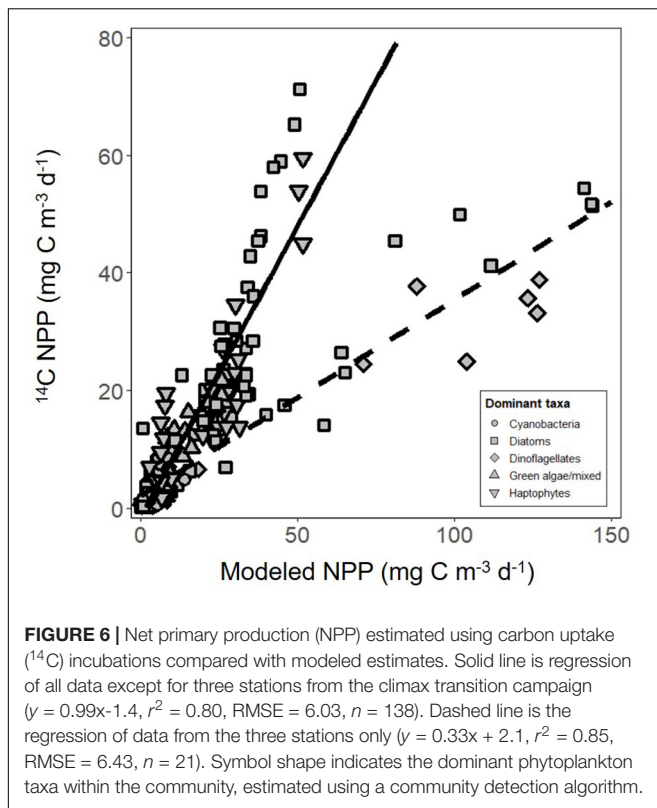
$n = 138$; **Figure 6**). Incubation values from three stations in the subarctic sampled during the climax transition also showed excellent agreement but had a markedly lower slope ($r^2 = 0.85$, $y = 0.33x + 2.1$, $\text{RMSE} = 6.43$, $n = 21$; **Figure 6**). Potential reasons for the apparent offset are discussed below. Nevertheless, modeled NPP consistently predicted measured values from discrete depths throughout the euphotic zone (**Figure 7**), confirming the ability of the model to capture depth-integrated estimates of NPP ($f\text{NPP}$).

Our analysis revealed clear trends in $f\text{NPP}$ and mixed layer μ ($f\mu$) over the annual bloom cycle and important differences in these properties between the subtropical and subarctic regions (**Figure 8** and **Table 3**). $f\text{NPP}$ was low during the *winter transition* in both regions, progressively increased during the *accumulation phase*, peaked during the *climax transition*, and declined in the *equilibrium phase* to values similar, or slightly higher, than the *winter transition* (**Figure 8A**). Across both regions and all phases of the annual bloom cycle, $f\text{NPP}$ was highest in the subarctic region during the *climax transition* (mean \pm s.d. = 1464 ± 440 , maximum = 2296, units = $\text{mg C m}^{-2} \text{ day}^{-1}$). $f\mu$ in the *winter transition* was markedly higher in the

subtropical region compared to the subarctic (mean 0.57 vs. 0.21; ANOVA, T-K, $p < 0.05$), but $f\text{NPP}$ in the *winter transition* was similar in these regions (**Figure 8C**). Thus, during winter, growth rate was the primary driver of NPP in the subtropical region, whereas the standing stock of phytoplankton carbon drove NPP in the subarctic region. $f\mu$ increased ~ 1.3 -fold between the *winter* and *climax transition* phases in the subtropical region but increased ~ 4 -fold over the same period in the subarctic region, achieving a similar mean of $\sim 0.75 \text{ day}^{-1}$ in both regions during the *climax transition*.

DISCUSSION

The ability to explain what drives spatio-temporal variability in phytoplankton productivity is essential for improving our understanding of global carbon dynamics. Early satellite-based approaches used Chl and predictive relationships with abiotic factors (e.g., light and temperature or nutrient concentration) to estimate depth-integrated productivity ($f\text{NPP}$) at a global scale (Platt and Sathyendranath, 1993; Antoine et al., 1996;



Behrenfeld and Falkowski, 1997a). Although these approaches could accurately predict $f\text{NPP}$, they could not address the sources of variability in physiology when compared to discrete field measurements, particularly the effects of photoacclimation on changes in cellular Chl [see Behrenfeld and Falkowski (1997b) and citations within]. More recently, phytoplankton growth was estimated using changes in Chl and C_{phyto} as a function of light, temperature, and nutrients (Behrenfeld et al., 2005), and a photoacclimation model (PaM) was developed independently to account for a deeper understanding of how phytoplankton regulate expression of Chl during deep mixing (Behrenfeld et al., 2016). Here, we show that NPP derived from PaM estimates of θ effectively captures both spatial (depth-resolved and regional scale) and temporal variability across the four NAAMES science-intensive campaigns.

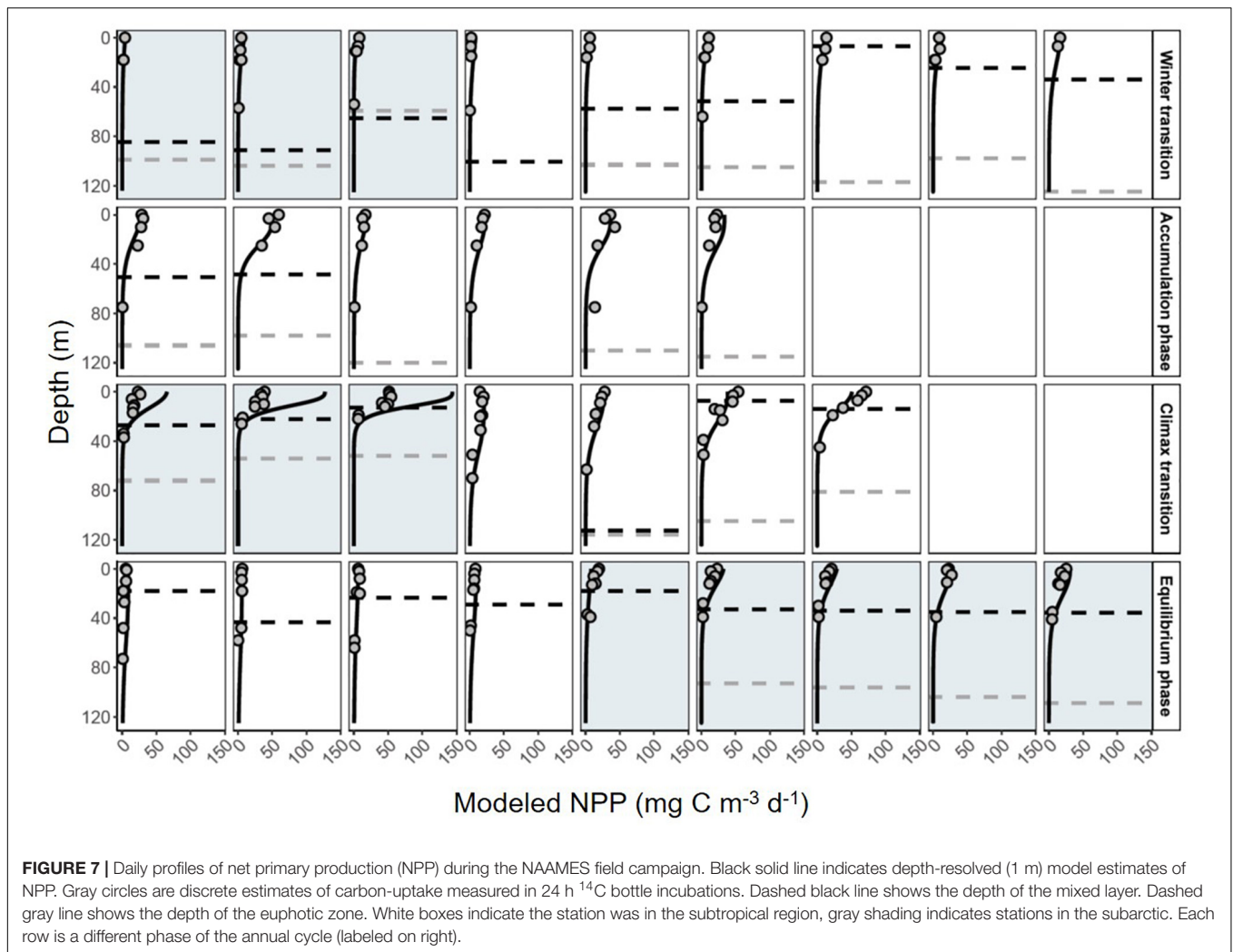
Environmental Controls on Phytoplankton Growth and Productivity

In situ estimates of phytoplankton μ and NPP in the North Atlantic bloom study region are relatively sparse. Rarely since the North Atlantic Bloom Experiment (NABE) of the Joint Global Ocean Flux Study (JGOFS) have both measurements been seen as integral to characterizing the annual cycles of phytoplankton bloom dynamics, resulting in a reliance on estimates derived from satellite, floats or models (Westberry et al., 2016; Briggs et al., 2018; Mignot et al., 2018). Although NABE was more limited in both spatial and temporal scope, it did capture the late spring bloom in the western North Atlantic during the same period of

time (April/May) as the NAAMES *climax transition* campaign. Despite a difference of almost 30 years between the two studies, the observations show very similar values. Model estimates of $f\text{NPP}$ from a comparable ($43^\circ \text{W } 44^\circ \text{N}$) site on the NAAMES transect ranged from 1139 to $1214 \text{ mg C m}^{-2} \text{ d}^{-1}$, and at the northern ($41^\circ \text{W } 45^\circ \text{N}$) NABE station estimates of $f\text{NPP}$ were $1140 \text{ mg C m}^{-2} \text{ d}^{-1}$ (Li et al., 1993). A slightly lower value of $1063 \text{ mg C m}^{-2} \text{ d}^{-1}$ was observed at the southern ($47^\circ \text{W } 40^\circ \text{N}$) station of NABE. This result conformed to previous findings that the bloom climax in this region ($\sim 45^\circ$) in the North Atlantic shows relatively low inter-annual variability either in time or magnitude (Henson et al., 2009; Uitz et al., 2010). Unique to this analysis of the NAAMES campaigns is the ship-based optical assessment of phytoplankton growth rate, which can help discern the abiotic and biological controls on the annual bloom cycle.

Phytoplankton growth, and consequently NPP, is a function of light, temperature and nutrients (Geider et al., 1998). While light harvesting is subject to a variety of strategies that ultimately dictate the maximal rate of division, the scarce availability of nutrients also requires physiological adjustments that involve highly efficient tuning of downstream carbon metabolism (MacIntyre et al., 2002; Halsey et al., 2010; Talmy et al., 2013). Phytoplankton strategies to optimize growth in response to light and nutrient availability appear to be shared by a diverse array of species, with distinct physiologies and evolutionary pathways (Halsey et al., 2013). The contrasting regimes of light and nutrient availability identified in the different regions in NAAMES resulted in distinct growth dynamics over the annual cycle. These behaviors have important implications for phytoplankton taxonomic succession, trophic energy transfer, and carbon export efficiency (the fraction of NPP exported out of the euphotic zone).

Three important differences were observed in the seasonal trends of $f\mu$ across the two regions that help explain regional differences in the magnitude of NPP. Firstly, $f\mu$ was substantially higher during the *winter transition* in the subtropical region compared to the subarctic. Second, median values of $f\mu$ were very similar across the two regions during the *bloom climax* phase. Third, the rate of change in $f\mu$ between the *winter transition* and *climax transition* was nearly 4-fold in the subarctic region, compared to 1.3-fold in the subtropical region (Figure 8C). The faster division rate measured in the subtropical region is unsurprising as the growth conditions encountered here during the four field campaigns were highly favorable: higher growth irradiance (I_g), greater physical stability of the water column, and moderate nutrient availability (except for the *equilibrium phase*; Supplementary Figures S2, S3). Thus, mean $f\mu$ was relatively stable throughout the annual cycle in the subtropical region and phytoplankton growth was only moderately light-limited during the *winter transition* (I_g of 0.11 ± 0.01 , mean \pm s.d; units = moles of photons $\text{m}^{-2} \text{ hr}^{-1}$) (Figure 8). In contrast, I_g in the subarctic *winter transition* was an order of magnitude lower (0.012 ± 0.006 moles of photons $\text{m}^{-2} \text{ hr}^{-1}$) than that observed in the subtropical region due to deeper mixing and, to a lesser extent, lower incident light. This appeared to result in severe light limitation, which inhibited growth in the surface layer and concurs with



previous findings from this region (Follows and Dutkiewicz, 2001; Henson et al., 2009).

The subtropical region defined in this study falls into a transition zone described by Henson et al. (2009), who concluded that phytoplankton in this region experience light and/or nutrient limitation. We found that $f\mu$ in the subtropical region remained relatively constant across the annual cycle, even with steadily decreasing N availability (Figure 9), suggesting that light, rather than nitrate or phosphate concentration (Supplementary Figures S2, S3), played the prevailing role in limiting growth. This idea is further supported by an increase in $f\mu$ during the *climax transition* when the shallow mixed layer increased light availability (I_g rose to 0.41 ± 0.35 moles of photons $\text{m}^{-2} \text{hr}^{-1}$ in spring). The conditions giving rise to this acceleration were also evident in the subarctic region, and the maximal mean growth rates observed across the two regions were similar (Figure 8). Nutrient availability (mainly N) only approached limiting concentrations in the subtropical region during the *equilibrium phase* (Figure 9). During this time $f\mu$ was almost identical to the values observed during periods of light limitation, while in the

subarctic $f\mu$ remained substantially higher than the values observed in winter.

Annual Bloom Dynamics in the Western North Atlantic

The stability of an ecosystem can strongly influence the diversity and survival strategy of the resident population (Tilman, 1996). Within the marine environment, stability is quite often a reference to physical properties, such as the strength of stratification which is inversely correlated to the rate of vertical mixing. Seasonal variability in stratification (or stabilization) of the water column is a key feature of many prominent phytoplankton bloom hypotheses (Sverdrup, 1953; Huisman et al., 1999; Behrenfeld and Boss, 2018), whilst “turbulence” is at the core of the current paradigm of taxonomic succession (Margalef, 1978). In the western North Atlantic, it could be argued that the two regions (subtropical and subarctic) offer contrasting regimes of ecosystem stability, which have a profound influence on the taxonomy, growth and productivity of the phytoplankton community, and in turn, carbon export.

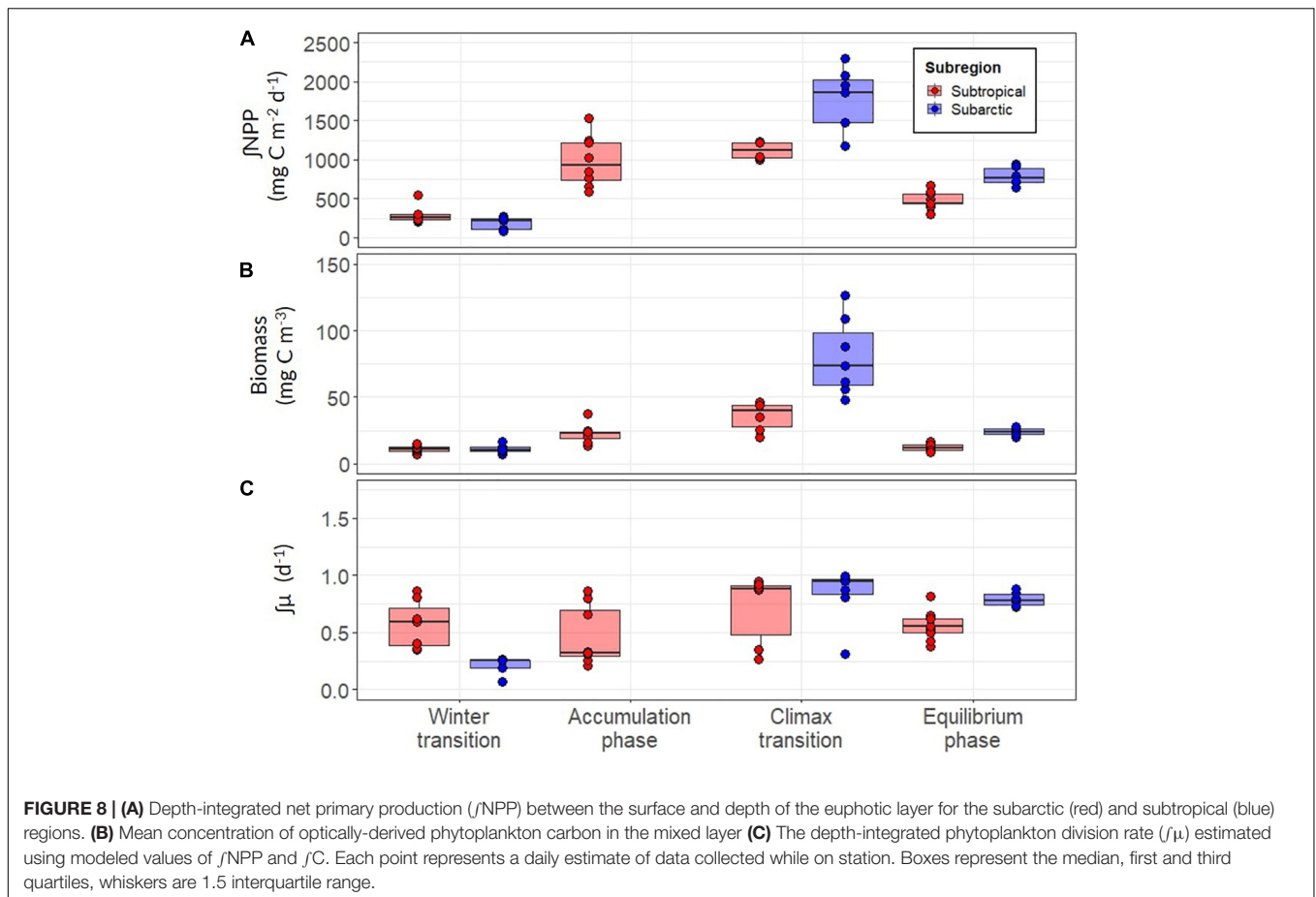


FIGURE 8 | (A) Depth-integrated net primary production (J_{NPP}) between the surface and depth of the euphotic layer for the subarctic (red) and subtropical (blue) regions. **(B)** Mean concentration of optically-derived phytoplankton carbon in the mixed layer **(C)** The depth-integrated phytoplankton division rate (J_{μ}) estimated using modeled values of J_{NPP} and J_C . Each point represents a daily estimate of data collected while on station. Boxes represent the median, first and third quartiles, whiskers are 1.5 interquartile range.

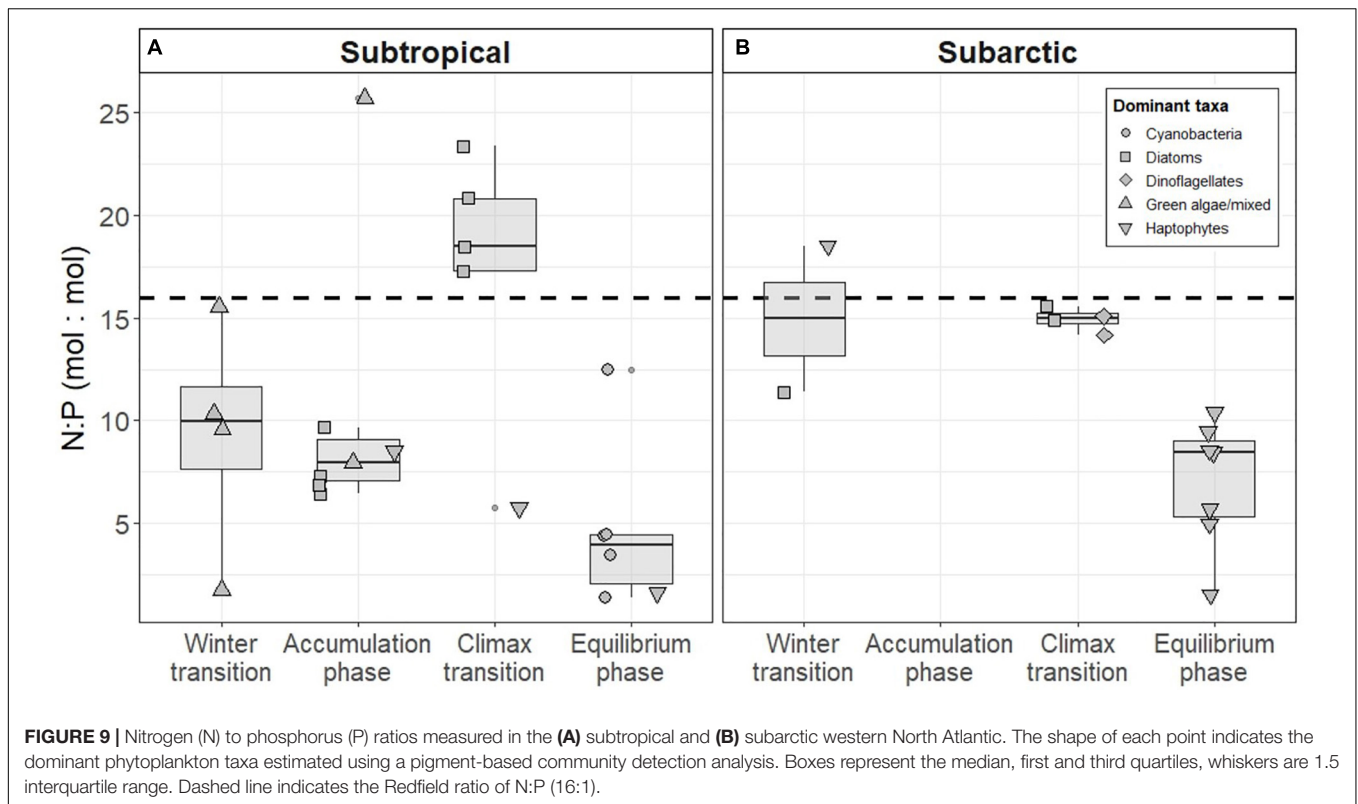
TABLE 3 | Mean and standard deviation, maximum and minimum values of net primary production (NPP) and phytoplankton division rate (μ) measured during the four NAAMES field campaigns.

	NAAMES 1 11/6/15–12/1/15 “winter transition”			NAAMES 4 03/20/18–4/13/18 “accumulation phase”			NAAMES 2 05/11/16–6/5/16 “climax transition”			NAAMES 3 08/30/17–9/24/17 “equilibrium phase”		
	Min	Max	Mean \pm SD	Min	Max	Mean \pm SD	Min	Max	Mean \pm SD	Min	Max	Mean \pm SD
NPP (^{14}C)	2.13	16.33	8.27 \pm 4.61	4.90	59.50	29.75 \pm 18.44	14.82	71.25	40.14 \pm 19.87	5.28	25.24	15.26 \pm 8.49
J_{μ}	0.07	0.86	0.41 \pm 0.24	0.21	0.87	0.46 \pm 0.26	0.26	0.99	0.77 \pm 0.27	0.37	0.88	0.65 \pm 0.15
J_{NPP}	78	550	248 \pm 116	593	1535	984 \pm 329	1004	2296	1464 \pm 440	297	945	602 \pm 192
$J_{NPP_{MLD}}$	72	425	205 \pm 96	226	1483	920 \pm 405	306	1960	1157 \pm 531	90	805	358 \pm 248

NPP (^{14}C), discrete estimates of NPP from ^{14}C bottle incubations; J_{μ} , modeled estimates of depth-integrated μ for the surface mixed layer; J_{NPP} , modeled estimates of depth-integrated NPP for the full euphotic zone; $J_{NPP_{MLD}}$, modeled estimates of depth-integrated NPP for the surface mixed layer.

The growth dynamics discussed in the previous section provide insight into factors that shape the annual cycle of phytoplankton biomass, particularly the magnitude and termination of a bloom. In the subtropical region, J_{μ} varied little over the annual cycle with only a small (1.3-fold) increase between the *winter transition* and *climax transition*. During this time, a more substantial (4-fold) change in biomass was observed as phytoplankton growth exceeded losses, leading to accumulation. The extent of accumulation, however, was significantly lower than the 7-fold change in biomass observed in the sub-arctic over the same period, during which the

acceleration of growth in this region was much faster. The differences between the two regions could be explained by a tight coupling of growth-loss processes in the subtropics, with significant accumulation quickly curtailed by recoupling of grazer control (amongst other loss processes) following a mild acceleration in phytoplankton growth. Such tight coupling was likely driven by the generally stable growth conditions (high light, shallow mixed layer) in the subtropical region that facilitated consistently high phytoplankton growth rates, which in turn provided a permanent food source for higher trophic levels (Banse, 2002). In contrast, stronger decoupling



from these loss processes likely occurred in the subarctic during the winter, when deeper vertical mixing resulted in more extreme light-limited growth conditions. Under such conditions, dilution of phytoplankton standing stocks would have reduced predator–prey encounter rates, resulting in a decline in predator abundance (Behrenfeld, 2014; Mayot et al., 2017). Collectively, these observations support the tenet of the Disturbance-Recoupling Hypothesis of bloom control, namely that the balance of phytoplankton growth and loss by predation determines bloom initiation and termination (Behrenfeld and Boss, 2018). The similar concentrations of biomass observed in the two regions during the *winter transition* is most likely explained by fewer, larger cells in the subarctic. Such divergent environments can result in very different strategies of survival and growth by the phytoplankton population, which can in turn influence the life cycles of key grazers that ultimately shape the development of a bloom (Friedland et al., 2016).

Regional Differences in Phytoplankton Community and the Implications for Carbon Export

Phytoplankton have evolved a number of growth strategies to increase competitive ability in environments of variable resource (light or nutrient) availability (Litchman and Klausmeier, 2008). Stable, stratified conditions such as those encountered in the subtropical region can often lead to phytoplankton communities dominated by taxonomic groups of smaller cell size (Finkel et al., 2010). Genetic profiling of phytoplankton community

composition from NAAMES revealed that this was also the case in the western North Atlantic, with the subtropical community generally dominated by picoeukaryotes and cyanobacteria during the *winter transition* and *climax transition* (Bolanos et al. in review). Pigment-based analysis also supports this finding and reveals that significant changes occurred in the subtropical phytoplankton community during different stages of the annual cycle (Figure 9). In the subtropical winter, green algae, potentially the picoeukaryotes identified in Bolanos et al. (in review), were prevalent during the *winter transition* before the community shifted to haptophytes and cyanobacteria during subsequent seasons. Communities dominated by picoplankton are typically associated with rapid carbon cycling by the microbial loop, a route that leads to lowered carbon export efficiency due to respiration losses incurred as particulate matter is processed through the trophic web of smaller zooplankton, ciliates and bacteria (Worden et al., 2015). In the comparably unstable conditions of the high latitudes, phytoplankton that possess an ability to grow rapidly in highly changeable conditions tend to prosper, leading to a more “classic” food chain (e.g., diatom-copepod-fish) often typical of upwelling and other productive regions (Schmoker et al., 2013). The larger phytoplankton cells that thrive in such conditions allow for more rapid sedimentation of particulate matter and increased export efficiency (Henson et al., 2019). Although only pigment-based composition of phytoplankton was considered in the study presented here, Imaging FlowCytobot data show both seasonal and regional differences in community composition. Nano-size cells (including diatoms <10 μm) dominated both subarctic and

subtropical communities during the *winter transition*, with high relative contributions of small diatoms to the total phytoplankton biovolume in the southernmost stations of the subtropical area of study. Whereas small cells continued to dominate communities in both subarctic and subtropical regions during the climax transition period, median cell size was higher in the subarctic region (Bolanos et al., in review).

A pronounced presence of prymnesiophytes and *Euglenida* (flagellates) in the subarctic during the *climax transition* (Bolanos et al., in review) may provide an important clue to explain the divergent slope in the modeled versus measured NPP relationship for the three stations occupied at this time (Figure 6). Bloom termination occurs as a result of recoupled phytoplankton growth and grazing pressure (Behrenfeld and Boss, 2018). It is conceivable that the 24 h dawn-to-dawn ^{14}C -incubations yielded markedly lower NPP values than the model estimates because ^{14}C -labeled C_{phyto} was rapidly recycled by grazers during the incubation. In fact, short term (2 h) ^{14}C -incubations performed midday on the same days as the 24 h ^{14}C -incubations during the *climax transition* in the subarctic gave carbon fixation rates that were among the highest measured across all campaigns (data not shown). This contrast between 2 h versus 24 h ^{14}C -incubations suggests that respiration of newly fixed C_{phyto} by the grazing community during the 24 h incubation caused measured NPP to appear ~ 3 -fold lower than the actual NPP rate.

CONCLUSION

The amount of carbon sequestered during a large phytoplankton bloom is ultimately driven by biomass rather than the division rate of the population, emphasized here during the *climax transition* of NAAMES. However, by examining differences in growth rate we are able to glean important information about the growth conditions and strategies implemented by the phytoplankton community as they adapt to the limitations imposed by their extant environment. If we are to further our understanding of global carbon cycling, more detailed knowledge of the spatial and temporal dynamics of phytoplankton division rate are required. Such an understanding of the physiological behaviors of diverse phytoplankton will not only provide insight into the resulting taxonomic composition of the phytoplankton

community but also resolve the grazing population and the predator-prey dynamics that notably dictate the fate of the fixed carbon.

DATA AVAILABILITY STATEMENT

The data presented are available from the SeaBASS data repository at <https://seabass.gsfc.nasa.gov/experiment/NAAMES>. Information concerning the collection and processing of inorganic nutrient samples are also available from SeaBASS. All scripts generated for this study are available on request from the corresponding author.

AUTHOR CONTRIBUTIONS

All authors contributed to either data collection, processing, or analysis. JF wrote the manuscript with guidance from KH and MB. All co-authors contributed to editing the manuscript.

FUNDING

This work was supported by NASA Grants NNX15AAF30G and 80NSSC17K568 to MB and NNX15AE70G to KH.

ACKNOWLEDGMENTS

We would like to thank the captain and crew of the R/V Atlantis for their support throughout the NAAMES field program. We would also like to thank all those who provided supporting data and Luis Bolanos who offered important insight into community composition dynamics.

SUPPLEMENTARY MATERIAL

The Supplementary Material for this article can be found online at: <https://www.frontiersin.org/articles/10.3389/fmars.2020.00024/full#supplementary-material>

REFERENCES

- Antoine, D., André, J.-M., and Morel, A. (1996). Oceanic primary production: 2. Estimation at global scale from satellite (Coastal Zone Color Scanner) chlorophyll. *Glob. Biogeochem. Cycles* 10, 57–69. doi: 10.1029/95gb02832
- Arrigo, K. (2005). Molecular diversity and ecology of microbial plankton. *Nature* 437, 349–355.
- Banse, K. (2002). Steemann Nielsen and the zooplankton. *Hydrobiologia* 480, 15–28.
- Behrenfeld, M. J. (2014). Climate-mediated dance of the plankton. *Nat. Clim. Change* 4, 880–887. doi: 10.1038/nclimate2349
- Behrenfeld, M. J., and Boss, E. S. (2014). Resurrecting the ecological underpinnings of ocean plankton blooms. *Annu. Rev. Mar. Sci.* 6, 167–194. doi: 10.1146/annurev-marine-052913-021325
- Behrenfeld, M. J., Boss, E., Siegel, D. A., and Shea, D. M. (2005). Carbon-based ocean productivity and phytoplankton physiology from space. *Global Biogeochem. Cycles* 19, 1–14.
- Behrenfeld, M. J., and Boss, E. S. (2018). Student's tutorial on bloom hypotheses in the context of phytoplankton annual cycles. *Glob. Change Biol.* 24, 55–77. doi: 10.1111/gcb.13858
- Behrenfeld, M. J., and Falkowski, P. G. (1997a). A consumer's guide to phytoplankton primary productivity models. *Limnol. Oceanogr.* 42, 1479–1491. doi: 10.4319/lo.1997.42.7.1479
- Behrenfeld, M. J., and Falkowski, P. G. (1997b). Photosynthetic rates derived from satellite-based chlorophyll concentration. *Limnol. Oceanogr.* 42, 1–20. doi: 10.4319/lo.1997.42.1.0001
- Behrenfeld, M. J., Moore, R. H., Hostetler, C. A., Graff, J., Gaube, P., Russell, L. M., et al. (2019). The North Atlantic Aerosol and marine ecosystem study (NAAMES): science motive and mission overview. *Front. Mar. Sci.* 6:122. doi: 10.3389/fmars.2019.00122
- Behrenfeld, M. J., O'Malley, R. T., Boss, E. S., Westberry, T. K., Graff, J. R., Halsey, K. H., et al. (2016). Reevaluating ocean warming impacts on global phytoplankton. *Nat. Clim. Change* 6, 323–330. doi: 10.1038/nclimate2838

- Behrenfeld, M. J., O'Malley, R. T., Siegel, D. A., McClain, C. R., Sarmiento, J. L., Feldman, G. C., et al. (2006). Climate-driven trends in contemporary ocean productivity. *Nature* 444, 752–755. doi: 10.1038/nature05317
- Behrenfeld, M. J., Westberry, T. K., Boss, E. S., O'Malley, R. T., Siegel, D. A., Wiggert, J. D., et al. (2009). Satellite-detected fluorescence reveals global physiology of ocean phytoplankton. *Biogeosciences* 6, 779–794. doi: 10.5194/bg-6-779-2009
- Bidle, K. D. (2015). The molecular ecophysiology of programmed cell death in marine phytoplankton. *Annu. Rev. Mar. Sci.* 7, 341–375. doi: 10.1146/annurev-marine-010213-135014
- Blondeau-Patissier, D., Gower, J. F. R. R., Dekker, A. G., Phinn, S. R., and Brando, V. E. (2014). A review of ocean color remote sensing methods and statistical techniques for the detection, mapping and analysis of phytoplankton blooms in coastal and open oceans. *Prog. Oceanogr.* 123, 123–144. doi: 10.1016/j.pcean.2013.12.008
- Boss, E., Swift, D., Taylor, L., Brickley, P., Zaneveld, R., Riser, S., et al. (2008). Observations of pigment and particle distributions in the western North Atlantic from an autonomous float and ocean color satellite. *Limnol. Oceanogr.* 53(5 Pt 2), 2112–2122. doi: 10.4319/lo.2008.53.5_part_2.2112
- Boss, E., Twardowski, M. S., and Herring, S. (2001). Shape of the particulate beam attenuation spectrum and its inversion to obtain the shape of the particulate size distribution. *Appl. Opt.* 40:4885. doi: 10.1364/ao.40.004885
- Boss, E. S., Collier, R., Larson, G., Fennel, K., and Pegau, W. S. (2007). Measurements of spectral optical properties and their relation to biogeochemical variables and processes in Crater Lake. Crater Lake National Park, OR. *Hydrobiologia* 574, 149–159. doi: 10.1007/978-1-4020-5824-0_9
- Boyd, P. W., Claustre, H., Levy, M., Siegel, D. A., and Weber, T. (2019). Multifaceted particle pumps drive carbon sequestration in the ocean. *Nature* 568, 327–335. doi: 10.1038/s41586-019-1098-2
- Bracher, A., Bouman, H. A., Brewin, R. J. W., Bricaud, A., Brotas, V., Ciotti, A. M., et al. (2017). Obtaining phytoplankton diversity from ocean color: a scientific roadmap for future development. *Front. Mar. Sci.* 4:55. doi: 10.3389/fmars.2017.00055
- Briggs, N., Guemundsson, K., Cetinić, I., D'Asaro, E., Rehm, E., Lee, C., et al. (2018). A multi-method autonomous assessment of primary productivity and export efficiency in the springtime North Atlantic. *Biogeosciences* 15, 4515–4532. doi: 10.5194/bg-15-4515-2018
- Burt, W. J., Westberry, T. K., Behrenfeld, M. J., Zeng, C., Izett, R. W., and Tortell, P. D. (2018). Carbon: chlorophyll ratios and net primary productivity of subarctic pacific surface waters derived from autonomous shipboard sensors. *Glob. Biogeochem. Cycles* 32, 267–288. doi: 10.1002/2017gb005783
- Cetinić, I., Perry, M. J., Briggs, N. T., Kallin, E., D'Asaro, E. A., and Lee, C. M. (2012). Particulate organic carbon and inherent optical properties during 2008 North Atlantic bloom experiment. *J. Geophys. Res. Oceans* 117:C06028.
- Cetinić, I., Poulton, N., and Slade, W. H. (2016). Characterizing the phytoplankton soup: pump and plumbing effects on the particle assemblage in underway optical seawater systems. *Opt. Express* 24:20703. doi: 10.1364/OE.24.020703
- Della Penna, A., and Gaube, P. (2019). Overview of (Sub)mesoscale ocean dynamics for the NAAMES field program. *Front. Mar. Sci.* 6:384. doi: 10.3389/fmars.2019.00384
- Estapa, M. L., Feen, M. L., and Breves, E. (2019). Direct observations of biological carbon export from profiling floats in the subtropical North Atlantic. *Glob. Biogeochem. Cycles* 33, 282–300. doi: 10.1029/2018gb006098
- Field, C. B., Behrenfeld, M. J., Randerson, J. T., and Falkowski, P. G. (1998). Primary production of the biosphere: integrating terrestrial and oceanic components. *Science* 281, 237–240. doi: 10.1126/science.281.5374.237
- Finkel, Z. V., Beardall, J., Flynn, K. J., Quigg, A., Rees, T. A. V., and Raven, J. A. (2010). Phytoplankton in a changing world: cell size and elemental stoichiometry. *J. Plankton Res.* 32, 119–137. doi: 10.1093/plankt/fbp098
- Follows, M., and Dutkiewicz, S. (2001). Meteorological modulation of the North Atlantic spring bloom. *Deep Sea Res. II Top. Stud. Oceanogr.* 49, 321–344. doi: 10.1016/s0967-0645(01)00105-9
- Friedland, K. D., Record, N. R., Asch, R. G., Kristiansen, T., Saba, V. S., Drinkwater, K. F., et al. (2016). Seasonal phytoplankton blooms in the North Atlantic linked to the overwintering strategies of copepods. *Elementa* 4:99.
- Geider, R., MacIntyre, H., and Kana, T. (1997). Dynamic model of phytoplankton growth and acclimation: responses of the balanced growth rate and the chlorophyll a:carbon ratio to light, nutrient-limitation and temperature. *Mar. Ecol. Prog. Ser.* 148, 187–200. doi: 10.3354/meps148187
- Geider, R. J., Delucia, E. H., Falkowski, P. G., Finzi, A. C., Grime, J. P., Grace, J., et al. (2001). Primary productivity of planet earth: biological determinants and physical constraints in terrestrial and aquatic habitats. *Glob. Change Biol.* 7, 849–882. doi: 10.1046/j.1365-2486.2001.00448.x
- Geider, R. J., MacIntyre, H. L., and Kana, T. M. (1998). A dynamic regulatory model of phytoplankton acclimation to light, nutrients, and temperature. *Limnol. Oceanogr.* 43, 679–694. doi: 10.4319/lo.1998.43.4.0679
- Giering, S. L. C., Sanders, R., Lampitt, R. S., Anderson, T. R., Tamburini, C., Boutrif, M., et al. (2014). Reconciliation of the carbon budget in the ocean's twilight zone. *Nature* 507, 480–483. doi: 10.1038/nature13123
- Graff, J. R., and Behrenfeld, M. J. (2018). Photoacclimation responses in Subarctic Atlantic phytoplankton following a natural mixing-restratification event. *Front. Mar. Sci.* 5:209. doi: 10.3389/fmars.2018.00209
- Graff, J. R., Westberry, T. K., Milligan, A. J., Brown, M. B., Dall'Olmo, G., van Dongen-Vogels, V., et al. (2015). Analytical phytoplankton carbon measurements spanning diverse ecosystems. *Deep Sea Res. I Oceanogr. Res. Pap.* 102, 16–25. doi: 10.1016/j.dsr.2015.04.006
- Halsey, K., Milligan, A., and Behrenfeld, M. (2014). Contrasting strategies of photosynthetic energy utilization drive lifestyle strategies in ecologically important picoeukaryotes. *Metabolites* 4, 260–280. doi: 10.3390/metabo4020260
- Halsey, K. H., and Jones, B. M. (2015). Phytoplankton strategies for photosynthetic energy allocation. *Annu. Rev. Mar. Sci.* 7, 265–297. doi: 10.1146/annurev-marine-010814-015813
- Halsey, K. H., Milligan, A. J., and Behrenfeld, M. J. (2010). Physiological optimization underlies growth rate-independent chlorophyll-specific gross and net primary production. *Photosynth. Res.* 103, 125–137. doi: 10.1007/s11120-009-9526-z
- Halsey, K. H., O'Malley, R. T., Graff, J. R., Milligan, A. J., and Behrenfeld, M. J. (2013). A common partitioning strategy for photosynthetic products in evolutionarily distinct phytoplankton species. *New Phytol.* 198, 1030–1038. doi: 10.1111/nph.12209
- Hemsley, V. S., Smyth, T. J., Martin, A. P., Frajka-Williams, E., Thompson, A. F., Damerell, G., and Painter, S. C. (2015). Estimating oceanic primary production using vertical irradiance and chlorophyll profiles from ocean gliders in the North Atlantic. *Environ. Sci. Technol.* 49, 11612–11621. doi: 10.1021/acs.est.5b00608
- Henson, S., Le Moigne, F., and Giering, S. (2019). Drivers of carbon export efficiency in the Global Ocean. *Glob. Biogeochem. Cycles* 33, 891–903. doi: 10.1029/2018gb006158
- Henson, S. A., Dunne, J. P., and Sarmiento, J. L. (2009). Decadal variability in North Atlantic phytoplankton blooms. *J. Geophys. Res. Oceans* 114:C04013.
- Huisman, J., van Oostveen, P., and Weissing, F. J. (1999). Critical depth and critical turbulence: two different mechanisms for the development of phytoplankton blooms. *Limnol. Oceanogr.* 44, 1781–1787. doi: 10.4319/lo.1999.44.7.1781
- Laws, E. A., and Bannister, T. T. (1980). Nutrient- and light-limited growth of *Thalassiosira fluviatilis* in continuous culture, with implications for phytoplankton growth in the ocean. *Limnol. Oceanogr.* 25, 457–473. doi: 10.4319/lo.1980.25.3.0457
- Li, W. K. W., Dickie, P. M., Harrison, W. G., and Irwin, B. D. (1993). Biomass and production of bacteria and phytoplankton during the spring bloom in the western North Atlantic Ocean. *Deep Sea Res. II Top. Stud. Oceanogr.* 40, 307–327. doi: 10.1016/0967-0645(93)90019-j
- Litchman, E., and Klausmeier, C. A. (2008). Trait-based community ecology of phytoplankton. *Annu. Rev. Ecol. Evol. Syst.* 39, 615–639. doi: 10.1146/annurev-ecolsys.39.110707.173549
- MacIntyre, H. L., Kana, T. M., Anning, T., and Geider, R. J. (2002). Photoacclimation of photosynthesis irradiance response curves and photosynthetic pigments in microalgae and cyanobacteria. *J. Phycol.* 38, 17–38. doi: 10.1046/j.1529-8817.2002.00094.x
- Margalef, R. (1978). Life-forms of phytoplankton as survival alternatives in an unstable environment. *Oceanol. Acta* 1, 493–509.
- Massicotte, P., Peeken, I., Katlein, C., Flores, H., Huot, Y., Castellani, G., et al. (2019). Sensitivity of phytoplankton primary production estimates to available irradiance under heterogeneous sea ice conditions. *J. Geophys. Res. Oceans* 124, 5436–5450. doi: 10.1029/2019jc015007
- Mayot, N., D'Ortenzio, F., Uitz, J., Gentili, B., Ras, J., Vellucci, V., et al. (2017). Influence of the phytoplankton community structure on the spring and annual

- primary production in the Northwestern Mediterranean Sea. *J. Geophys. Res. Oceans* 122, 9918–9936. doi: 10.1002/2016jc012668
- Mignot, A., Ferrari, R., and Claustre, H. (2018). Floats with bio-optical sensors reveal what processes trigger the North Atlantic bloom. *Nat. Commun.* 9, 1–9.
- Moore, C. M., Mills, M. M., Arrigo, K. R., Berman-Frank, I., Bopp, L., Boyd, P. W., et al. (2013). Processes and patterns of oceanic nutrient limitation. *Nat. Geosci.* 6, 701–710.
- Morel, A., Huot, Y., Gentili, B., Werdell, P. J., Hooker, S. B., and Franz, B. A. (2007). Examining the consistency of products derived from various ocean color sensors in open ocean (Case 1) waters in the perspective of a multi-sensor approach. *Remote Sens. Environ.* 111, 69–88. doi: 10.1016/j.rse.2007.03.012
- O'Reilly, J. E., Maritorena, S., Mitchell, B. G., Siegel, D. A., Carder, K. L., Garver, S. A., et al. (1998). Ocean color chlorophyll algorithms for SEAWIFS. *J. Geophys. Res. Oceans* 103, 24937–24953. doi: 10.1029/98jc02160
- Platt, T., and Sathyendranath, S. (1993). Estimators of primary production for interpretation of remotely sensed data on ocean color. *J. Geophys. Res.* 98, 14561–14576.
- Rowe, G. T., Sibuet, M., Deming, J., Tietjen, J., and Khrifounoff, A. (1990). Organic carbon turnover time in deep-sea benthos. *Prog. Oceanogr.* 24, 141–160. doi: 10.1371/journal.pone.0063796
- Sanders, R., Henson, S. A., Koski, M., De La Rocha, C. L., Painter, S. C., Poulton, A. J., et al. (2014). The biological carbon pump in the North Atlantic. *Prog. Oceanogr.* 129, 200–218. doi: 10.1016/j.pocean.2014.05.005
- Schmoker, C., Hernández-León, S., and Calbet, A. (2013). Microzooplankton grazing in the oceans: impacts, data variability, knowledge gaps and future directions. *J. Plankton Res.* 35, 691–706. doi: 10.1093/plankt/fbt023
- Siegel, D. A., Buesseler, K. O., Behrenfeld, M. J., Benitez-Nelson, C. R., Boss, E., Brzezinski, M. A., et al. (2016). Prediction of the export and fate of global ocean net primary production: the EXPORTS science plan. *Front. Mar. Sci.* 3:22. doi: 10.3389/fmars.2016.00022
- Siegel, D. A., Buesseler, K. O., Doney, S. C., Sailley, S. F., Behrenfeld, M. J., and Boyd, P. W. (2014). Global assessment of ocean carbon export by combining satellite observations and food-web models. *Glob. Biogeochem. Cycles* 28, 181–196. doi: 10.1002/2013gb004743
- Silsbe, G. M., Behrenfeld, M. J., Halsey, K. H., Milligan, A. J., and Westberry, T. K. (2016). The CAFE model: a net production model for global ocean phytoplankton. *Glob. Biogeochem. Cycles* 30, 1756–1777. doi: 10.1002/2016gb005521
- Slade, W. H., Boss, E., Dall'olmo, G., Langner, M. R., Loftin, J., Behrenfeld, M. J., et al. (2010). Underway and moored methods for improving accuracy in measurement of spectral particulate absorption and attenuation. *J. Atmos. Ocean. Technol.* 27, 1733–1746. doi: 10.1175/2010jtecho755.1
- Smyth, T. J., Tilstone, G. H., and Groom, S. B. (2005). Integration of radiative transfer into satellite models of ocean primary production. *J. Geophys. Res. C Oceans* 110, 1–11.
- Sverdrup, H. U. (1953). On conditions for the vernal blooming of phytoplankton. *ICES J. Mar. Sci.* 18, 287–295. doi: 10.1093/icesjms/18.3.287
- Talmy, D., Blackford, J., Hardman-Mountford, N. J., Dumbrell, A. J., and Geider, R. J. (2013). An optimality model of photoadaptation in contrasting aquatic light regimes. *Limnol. Oceanogr.* 58, 1802–1818. doi: 10.4319/lo.2013.58.5.1802
- Tilman, D. (1996). Biodiversity: population versus ecosystem stability. *Ecology* 77, 350–363. doi: 10.2307/2265614
- Uitz, J., Claustre, H., Gentili, B., and Stramski, D. (2010). Phytoplankton class-specific primary production in the world's oceans: seasonal and interannual variability from satellite observations. *Glob. Biogeochem. Cycles* 24, 1–19.
- Van Heukelem, L., and Thomas, C. S. (2001). Computer-assisted high-performance liquid chromatography method development with applications to the isolation and analysis of phytoplankton pigments. *J. Chromatogr. A* 910, 31–49. doi: 10.1016/s0378-4347(00)00603-4
- Westberry, T., Behrenfeld, M. J., Siegel, D. A., and Boss, E. (2008). Carbon-based primary productivity modeling with vertically resolved photoacclimation. *Glob. Biogeochem. Cycles* 22, 1–18.
- Westberry, T. K., Schultz, P., Behrenfeld, M. J., Dunne, J. P., Hiscock, M. R., Maritorena, S., et al. (2016). Annual cycles of phytoplankton biomass in the subarctic Atlantic and Pacific Ocean. *Glob. Biogeochem. Cycles* 30, 175–190. doi: 10.1002/2015gb005276
- Worden, A. Z., Follows, M. J., Giovannoni, S. J., Wilken, S., Zimmerman, A. E., and Keeling, P. J. (2015). Rethinking the marine carbon cycle: factoring in the multifarious lifestyles of microbes. *Science* 347:1257594. doi: 10.1126/science.1257594
- Zhang, B., and Horvath, S. (2005). A general framework for weighted gene co-expression network analysis. *Stat. Applicat. Genet. Mol. Biol.* 4:17.

Conflict of Interest: The authors declare that the research was conducted in the absence of any commercial or financial relationships that could be construed as a potential conflict of interest.

Copyright © 2020 Fox, Behrenfeld, Haëntjens, Chase, Kramer, Boss, Karp-Boss, Fisher, Penta, Westberry and Halsey. This is an open-access article distributed under the terms of the Creative Commons Attribution License (CC BY). The use, distribution or reproduction in other forums is permitted, provided the original author(s) and the copyright owner(s) are credited and that the original publication in this journal is cited, in accordance with accepted academic practice. No use, distribution or reproduction is permitted which does not comply with these terms.